This is a preprint, the final version is subject to change, of the American Mineralogist (MSA)
Cite as Authors (Year) Title. American Mineralogist, in press.
(DOI will not work until issue is live.) DOI: http://dx.doi.org/10.2138/am-2016-5335

Revision 2

Elastic wave velocities in polycrystalline $Mg_3Al_2Si_3O_{12}$-pyrope garnet to 24 GPa and 1300K

Julien Chantel[1,†,*] Geeth M. Manthilake[1], Daniel J. Frost[2], Christopher Beyer[2], Tiziana Boffa Ballaran[2], Zhicheng Jing[3,†], Yanbin Wang[3]

[1] Laboratoire magmas et volcans, CNRS, UMR 6524, IRD, Université Blaise Pascal, 63038 Clermont-Ferrand, France

[2] Bayerisches Geoinstitut, University Bayreuth, 95447 Bayreuth, Germany

[3] Center for Advanced Radiation Source, The University of Chicago, Chicago, IL 60637, USA

[†] Now at Department of Earth, Environmental and Planetary Sciences, Case Western Reserve University, Cleveland, OH 44106, USA

* Corresponding author: julien.chantel@case.edu

Correspondence to:

Julien Chantel

Department of Earth, Environmental, and Planetary Sciences

Case Western Reserve University

214 A.W. Smith Bldg.

10900 Euclid Ave.

Cleveland, OH 44106, USA

Phone: (216) 368-1903

Fax: (216) 368-3691

julien.chantel@case.edu

Abstract

The mantle transition zone, at depths between 410 to 660 km, is characterized by two prominent discontinuities in seismic-wave velocity in addition to a relatively steep velocity gradient. Throughout this region garnet will be an abundant mineral, the composition of which will change depending on both depth and lithology. It is important, therefore, to be able to characterize the effects of these changes on seismic velocities, which means that models must incorporate reliable elasticity data on the dominant mineral end-members that can be accurately employed at mantle conditions.

In this study elastic wave velocities of synthetic polycrystalline pyrope garnet ($Mg_3Al_2Si_3O_{12}$) have been measured using ultrasonic interferometry combined with energy-dispersive synchrotron X-ray diffraction in a 1000-ton multi-anvil press. Measurements were performed at pressures up to 24 GPa, conditions compatible with the base of the transition zone, and at temperatures up to 1300K. Least squares refinement of the ambient temperature data to a 3rd order finite strain equation yields values for the bulk and shear moduli and their pressure derivatives of K_{S0} = 172.0±1.6 GPa, G_0 = 89.1±0.5 GPa, $\delta K_S / \delta P$ = 4.38 ±0.08 and $\delta G / \delta P$ = 1.66 ±0.05. The determined temperature derivatives are $\delta K_S / \delta T$ = -17.8±2.0 MPa/K and $\delta G / \delta T$ = -7.9±1.0 MPa/K. High temperature data were fitted to extract parameters for a thermodynamic model. As several high pressure and temperature studies have been performed on pyrope, fitting all of the available data provides a more robust assessment of the accuracy of velocity measurements and allows the uncertainties that are inherent in the various methodologies to be realized. When this model is used to determine pyrope velocities at transition zone conditions the propagated uncertainties are approximately 1.5 and 2.5 % for V_p and V_s respectively. In order to reduce these uncertainties it is important not only to measure velocities as close as possible to mantle temperatures but also to understand what causes the difference in velocities between studies. Pyrope V_p and V_s at mantle transition zone conditions are found to be approximately 2.4 % and 3.7 %, respectively, larger than recent determinations of majoritic garnet at the same conditions, implying a significant variation with chemistry that is mainly realized at high temperatures.

Keywords: Elasticity; pyrope; equation of state; synchrotron radiation; ultrasonic interferometry.

Introduction

Experiment-based models for the mineralogy of the mantle indicate that garnet is a major constituent of both the upper mantle and transition zone and its stability extends into the top 100 km of the lower mantle (Anderson and Bass 1984; Irifune and Ringwood 1987; Weidner and Ito 1987; Duffy and Anderson 1989; Ita and Stixrude 1992). In the mid transition zone garnet comprises ~40 vol% of a bulk silicate Earth (BSE) or ultramafic composition and up to 70 vol% of a mafic composition. $Mg_3Al_2Si_3O_{12}$ pyrope is the principal component in garnet formed from a BSE composition in the upper mantle but by transition zone pressures it becomes subordinate to the $Mg_4Si_4O_{12}$-majorite component (Irifune and Ringwood 1987). Majorite forms as pyroxenes breakdown and Mg and Si substitute into the octahedrally coordinated Al site of garnet. However, at the base of the transition zone and in the lower mantle the exsolution of $CaSiO_3$ perovskite and the formation of bridgmanite drive the garnet composition to be pyrope-rich once more (Nishihara and Takahashi 2001; Saikia et al. 2008). As a consequence of the high abundance of garnet in the mantle and the significance of the pyrope component, experimental studies on the elasticity of this end member are important for the interpretation of seismic velocities throughout the top 750 km of the mantle (Bass and Anderson 1984; Duffy and Anderson 1989; Cammarano et al. 2003; Li and Liebermann 2007).

Many earlier studies of the elastic properties of pyrope were performed at ambient temperature (Chen et al. 1999; Conrad et al. 1999; Sinogeikin and Bass 2000) or at ambient pressure and high temperatures (Sumino and Nishizawa 1978; Suzuki and Anderson 1983; Sinogeikin and Bass 2002). Recent ultrasonic measurements of the sound velocities of polycrystalline pyrope have been reported up to 9 GPa and 1300K (Gwanmesia et al. 2006, 2007) and 20 GPa and 1700K (Zou et al. 2012). However, to date no studies have extended to the pressures and temperatures of the lower mantle where the pyrope end member becomes once more dominant in garnet (Nishihara and Takahashi 2001).

In this paper, we report new measurements of the elastic compressional (*P*) and shear (*S*) wave

velocities for synthetic polycrystalline pyrope [Py_{100} = $Mg_3Al_2Si_3O_{12}$] determined by ultrasonic interferometry to simultaneous pressures and temperatures of 24 GPa and 1300K, in conjunction with measurements of density and sample length by synchrotron X-ray diffraction and X-ray radiography. We have evaluated high pressure and temperature effects on the sound velocities of garnet and we use these to interpret seismic wave velocities of the mantle.

Experimental techniques

Sample synthesis and characterization

The starting material was a homogeneous glass of pyrope ($Mg_3Al_2Si_3O_{12}$) composition, prepared from dried reagent grade MgO, SiO_2 and Al_2O_3. The crushed glass was densely packed into a capsule fabricated from 0.025 mm thick rhenium foil that was initially 2 mm in diameter and 2.7 mm long. The capsule was inserted into a 14 mm edge length Cr_2O_3-doped MgO octahedral pressure assembly that employed internal MgO spacers and a stepped $LaCrO_3$ heater. Throughout the experiment, the temperature was monitored with a $W_{97}Re_3$–$W_{75}Re_{25}$ thermocouple, the junction of which was placed near the capsule. The assembly was compressed using a 1500-ton uniaxial, split-sphere multianvil apparatus (LP1500) (Laboratoire Magmas et Volcans, Clermont-Ferrand, France), employed tungsten carbide cubes with 8 mm long corner truncations. The polycrystalline sample (run #112) was synthesized at 10 GPa and 1300K by heating for 1h and following the compression and heating cycle described by Gwanmesia et al. (1993). The recovered sample was approximately 2 mm long and 1.2 mm in diameter. Synchrotron source x-ray diffraction of the recovered sample yielded a pattern that was consistent with the presence of pyrope only (JCPDS file no.150742). Complete transformation from the starting material to crystalline pyrope was inferred, as the pattern also displayed no broad background that would be indicative of residual glass. The surface of the recovered sample was analyzed using a LEO Gemini 1530 scanning electron microscope (Bayerisches Geoinstitut, Bayreuth, Germany) to determine the chemical purity and grain size, which was < 10 μm (Figure 1). Electron back scattered diffraction (EBSD) of the recovered sample

101 revealed no preferential orientation. In preparation for the ultrasonic measurements, the ends of the
102 cylindrical sample, as well as those of a dense alumina buffer rod, were ground and polished to a parallel
103 and flat finish with 6, 3, and 1 μm diamond polishing compounds. The final sample was a cylinder with a
104 thickness of 460 μm and a length to diameter ratio smaller than 0.5, in order to avoid reflection of the
105 acoustic echo from the sides of the sample and to facilitate detection of the compressional wave arrivals.
106
107 **Data collection**
108 A combination of *in situ* X-ray methods and ultrasonic velocity measurements were conducted at
109 the 13-ID-D beamline of GSECARS at the Advanced Photon Source, Argonne, IL, USA, using a 1000-
110 ton press and a double-stage multi-anvil module (T-25, Wang et al. 2009). A 10 mm edge length Cr_2O_3-
111 doped MgO octahedral pressure assembly was employed with tungsten carbide cubes that had 4 mm edge
112 length corner truncations. A cylindrical rhenium foil furnace that contained two opposing, laser-cut,
113 windows to facilitate X-ray transparency (Chantel et al. 2012) was placed inside the assembly. The
114 sample was centered inside the furnace within a sleeve of MgO. One end of the sample was directly in
115 contact with the dense alumina buffer rod used to transmit the ultrasonic signal, while the opposite end of
116 the sample was backed by a softer NaCl pellet (Supplementary Figure 1). Gold foils, 2 μm thick, were
117 placed at both ends of the sample to enhance acoustic bonding and to function as visual markers for the
118 sample length measurements obtained using X-ray radiographic imaging (Supplementary Figure 2).
119 Throughout the experiment, the temperature was monitored with a $W_{97}Re_3$–$W_{75}Re_{25}$ thermocouple,
120 the junction of which was in contact with an MgO spacer 0.5 mm in thickness, the other side of which
121 was in contact with the pressure marker (Supplementary Figure 1). Pressure was monitored using
122 measurements of the unit-cell volumes of Au, NaCl and MgO employing the equations of state of Fei et
123 al. (2004) and Matsui et al. (2012), respectively. Powder X-ray diffraction data from the sample and the
124 pressure markers were collected using in energy-dispersive geometry at a diffraction angle of 6.09°. A
125 YAG phosphor crystal was placed in the beam path behind the sample to convert the X-ray absorption

126 contrast of the assembly into visible light. A charge-coupled device (CCD) was used to record images for
127 sample length measurement at high-resolution (1 pixel ≈ 2 μm).

128 Ultrasonic velocity measurements were conducted simultaneously with *in situ* X-ray observations.
129 The travel times of both *P* and *S* waves were determined using a Tektronix Digital Oscilloscope using the
130 pulse–echo method at three selected frequencies (30, 40 and 50 MHz) (Papadakis 1990). The data
131 acquisition time at each pressure and temperature point was typically 5 min. All data reported were
132 collected during the cooling and decompression cycles to ensure the release of non-hydrostatic stresses
133 that may have arisen during cold compression (Supplementary Figure 3). The uncertainties of the velocity
134 measurements are within 0.5% in both V_P and V_S at ambient temperature (Chantel et al 2012). The major
135 contribution to this uncertainty comes from the determination of the sample length, which is in the range
136 0.2 – 0.4%, while the uncertainty on the travel-time is only 0.1%. Specimen lengths at high *P* and *T* were
137 calculated from the original sample length, compared against lengths obtained from the x-ray
138 radiographic images collected at all conditions. The temperature uncertainty is estimated to be
139 approximately 8% at 1300 K, which would correspond to an additional velocity uncertainty of
140 approximately 0.3% in V_P and 0.5% in V_S at 1300 K. At 800 K these thermally induced errors are
141 approximately half.
142
143 **Results**

144 Energy dispersive powder X-ray diffraction patterns were processed using full profile LeBail
145 refinements with the *Jana2006* software package (Petricek et al. 2006). Patterns for the sample, collected
146 over the entire range of pressure and temperature investigated were indexed in the $Ia\bar{3}d$ space group. No
147 evidence for the presence of additional phases was observed throughout the experiment. The lattice
148 parameter and unit cell volume at different *P-T* conditions were determined from the *in situ* X-ray
149 diffraction data. The corresponding densities are reported in Table 1 with the pressure from both the Au
150 calibrant (Fei et al. 2004) and that refined using the density and bulk modulus determined from our

151 measurements (i.e. absolute pressures, see later). The zero pressure density ρ_0, determined within the
152 multianvil before the samples was compressed, was 3.565 (5) g.cm^{-3}, which is in good agreement with the
153 bench top measurement of 3.56 g.cm^{-3}, obtained using the Archimedes' immersion method, and with
154 determinations of previous studies, i.e. 3.566 (1), 3.57 and 3.56 (2) g.cm^{-3}, respectively from Zou et al.
155 (2012), Sinogeikin and Bass (2002) and Gwanmesia et al. (2006).

156 The travel times for both longitudinal and shear waves and densities were measured to 24 GPa and
157 1300K. The measured velocities are plotted as a function of pressure in Figure 2 and compared with
158 similar multianvil ultrasonic measurements performed by Chen et al. (1999), Gwanmesia et al. (2006,
159 2007) and Zou et al. (2012) and single crystal Brillouin results of Sinogeikin and Bass (2000) obtained in
160 the diamond anvil cell. Values of V_P and V_S measured for pyrope in this study increase near linearly with
161 pressure. Longitudinal velocities determined in this study are in excellent agreement with those reported
162 by Gwanmesia et al. (2006, 2007) and Zou et al. (2012), while those of Chen et al. (1999) measured up to
163 ~10 GPa have larger values and the velocities measured by Sinogeikin and Bass (2000) are up to ~2 %
164 smaller. The shear wave velocities measured in this study are, on the other hand, in good agreement with
165 the measurements of Gwanmesia et al. (2006, 2007) and Sinogeikin and Bass (2000) but are up to ~1.5 %
166 smaller than values reported by Zou et al. (2012) and Chen et al. (1999). These discrepancies are
167 significantly outside of the uncertainties reported by the individual data sets and it is difficult to assess
168 their origin since it may arise from systematic errors inherent to the different measurements. However, a
169 possible explanation at least for the larger velocities reported by Chen et al. (1999) may be the
170 development of non-hydrostatic stress upon cold compression, as suggested by Gwanmesia et al. (2006).

171 Adiabatic elastic properties can be extracted from volume measurements and compressional (V_P)
172 and shear (V_S) velocity data, independently of X-ray pressure determinations. This is generally performed
173 using finite strain equations based on a 4th order expansion of the Helmholtz free energy (Davies and
174 Dziewonski 1975; Li and Zhang 2005), expressed in the form:

$$\rho V_P^2 = (1-2\varepsilon)^{5/2}(L1 + L2\varepsilon + \frac{1}{2}L3\varepsilon^2) \quad (1)$$

$$\rho V_S^2 = (1-2\varepsilon)^{5/2}(M1 + M2\varepsilon + \frac{1}{2}M3\varepsilon^2) \quad (2)$$

where ε is the eulerian finite strain: $\varepsilon = \frac{1}{2}\left[1 - \left(\frac{\rho}{\rho_0}\right)^{2/3}\right]$, and $L1$, $L2$, $L3$, $M1$, $M2$ and $M3$ are expressed in terms of the zero pressure values of shear and bulk moduli, G_0 and K_{S0}, and their first and second pressure derivatives, K'_0, G'_0, K''_0, and G''_0:

$$L1 = K_{S0} + \frac{4}{3}G_0 \quad (3)$$

$$L2 = 5(K_{S0} + \frac{4}{3}G_0) - 3K_{S0}(K'_0 + \frac{4}{3}G'_0) \quad (4)$$

$$L3 = 35\left(K_{S0} + \frac{4}{3}G_0\right) + 9K_{S0}(K'_0 - 4)\left(K'_0 + \frac{4}{3}G'_0\right) + 9K_{S0}^2\left(K''_0 + \frac{4}{3}G''_0\right) \quad (5)$$

$$M1 = G_0 \quad (6)$$

$$M2 = 5G_0 - 3K_{S0}G'_0 \quad (7)$$

$$M3 = 35G_0 + 9(K'_0 - 4)K_{S0}G'_0 + 9K_{S0}^2G''_0 \quad (8)$$

Expressions (1) and (2) are normally truncated at 3rd order by simply neglecting the ε^2 parameters. The experimental data are then fitted using the resulting two linear expressions:

$$\rho V_P^2 = (1-2\epsilon)^{5/2}(L1 + L2\varepsilon) \quad (9)$$

$$\rho V_S^2 = (1-2\epsilon)^{5/2}(M1 + M2\varepsilon) \quad (10)$$

and the ambient pressure adiabatic shear and bulk moduli and their first pressure derivatives are obtained from:

$$G_0 = M1 \quad (11)$$

$$K_{S0} = L1 - \frac{4}{3}G_0 \quad (12)$$

194 $$G'_0 = \frac{1}{3}(5M1 - M2)/K_{S0} \quad (13)$$

195 $$K'_{S0} = \frac{1}{3}(5L1 - L2)/K_{S0} - \frac{4}{3}G'_0 \quad (14)$$

196 The pressure at each data point is determined using,

197 $$P = -(1-2\varepsilon)^{5/2}(C_1\varepsilon + 0.5C_2\varepsilon^2) \quad (15)$$

198 where $C_1 = 3L_1 - 4M_1$ and $C_2 = 3L_2 - 4M_2 + 7C_1$. We refer to this as the absolute pressure as it is
199 determined independently of a secondary pressure standard.

200 When the data from this study are fitted to equations 9 and 10 values of 89.3±0.5, 171.4 ±1.6, 1.64 ±0.05
201 and 4.49 ±0.08 are obtained for G_0 and K_{S0} and their pressure derivatives, respectively. If the 4th order
202 expression were retained then the coefficients L3 and M3 would equate to expressions involving G''_0 and
203 K''_0, the second derivatives of G and K with respect to pressure, as shown in equations 5 and 8. The
204 precision of the majority of high-pressure data is not sufficient to constrain such quantities. If the current
205 data are fitted with the 4th order expression, for example, the quality of fit compared to the 3rd order fitting
206 does not improve but values for K'_0 and G'_0 of 1.66 and 0.95 are obtained, which are physically
207 unrealistic, and result in implausible behavior upon even minor extrapolation.
208
209 It is interesting to note, however, that expressions (9) and (10), do not include the complete derivatives of
210 the 3rd order expansion of the Helmholtz free energy. Considering such complete derivatives results in
211 velocities that still depend on ε^2 (Sammis et al. 1970) i.e.:

212 $$\rho V_P^2 = (1-2\varepsilon)^{5/2}(L1 + L2\varepsilon + L^*\varepsilon^2) \quad (16)$$

213 $$\rho V_S^2 = (1-2\varepsilon)^{5/2}(M1 + M2\varepsilon + M^*\varepsilon^2) \quad (17)$$

214 where M^* and L^* are defined as:

215 $$M^* = -24K_{S0} + \frac{9}{2}K_{S0}K'_0 - 4M1 - 2M2 \quad (18)$$

$$L^* = -72K_{S0} - 18K_0G'_0 + \frac{37}{2}L1 - \frac{13}{2}L2 \quad (19)$$

Note that the parameters in ε^2, i.e. L^* and M^*, resulting from deriving the 3rd order truncation of the Helmholtz energy do not include the moduli second derivatives that would be present in the 4th order truncation (equations 5 and 8). Sammis et al. (1970) concluded, therefore, that the ε^2 parameters resulting from the 3rd order truncation being incomplete, should be ignored. However, their inclusion in recent models (Stixrude and Lithgow-Bertelloni 2005) means they should be at least considered for internal consistency. When the data from this study are fitted by considering equation 16 and 17, then values of 89.1±0.5, 172±1.6, 1.66 ±0.05 and 4.38 ±0.08 for G_0, K_{S0} and their pressure derivatives, are obtained respectively. The differences between these values and those obtained using equations 9 and 10 instead are indeed small, but for K'_0, which decreases by ~2.5 %, the difference is larger than the uncertainty. Moreover once the elastic parameters obtained considering the full 3th order truncation of the Helmholtz energy are used in the model of Stixrude and Lithgow-Bertelloni (2005), the experimental V_P and V_S data are actually better reproduced than when using the parameters obtained through equations 9 and 10.

The elastic moduli and their derivatives determined using both the complete and incomplete 3rd order expressions fall within the range of values reported by previous studies on pyrope (Table 2). Between this and previous studies, however, no single set of consistent values for these parameters arises, within the reported uncertainties. This implies that in addition to the fitting uncertainties, which are normally reported, there must be further experimental uncertainties inherent in the techniques employed. One way to assess these uncertainties, and to determine the most appropriate set of moduli and derivatives, is by fitting all the available data simultaneously. If complete 3rd order fitting is performed on all data from the 3 studies, in addition to this one, that have measured velocities and densities simultaneously (Sinogeikin and Bass 2000; Gwanmesia et al. 2006; Zou et al. 2012) then the values 91.4

240 ±0.6, 170.6 ±2.7, 1.55 ±0.1 and 4.36 ±0.2 for G_0, K_{S0} and their pressure derivatives, are obtained
241 respectively. This "global" fitting of all appropriate data sets must provide a more realistic assessment of
242 the accuracy in elastic properties for what appears to be one of the most well studied mineral components.
243 A 2 dimensional fit to the high temperature data collected in this study yields the temperature
244 derivative $\partial Ks/\partial T$ = -17.8±2.0 and $\partial G/\partial T$ = -7.9±1.0 MPa/K. The latter value is slightly smaller than
245 previous estimates (Table 2). This may be due to the fact that this parameter decreases with pressure and
246 the high temperature data collected in this study are biased by higher pressures compared to other studies,
247 although it cannot be excluded that such a value is not well constrained due to the restricted number of
248 high temperature data available. The ambient and high temperature data are shown in Figure 3 along with
249 a fit performed only on our data using the thermo-elastic model of Stixrude and Lithgow-Bertelloni
250 (2005) (Table 3). This model employs a 3rd order Eulerian finite strain formulation to describe the effects
251 of cold compression, while the thermal contribution is obtained through a Mie-Grüneisen formalism. In
252 addition to the (isothermal) cold compression parameters G_0, K_{T0}, G'_0 and K'_0, the thermal part of the
253 equation of state employs the parameters θ, γ_0, q and η_0 (Stixrude and Lithgow-Bertelloni 2005), which
254 are respectively the Debye temperature, the Grüneisen parameter, the logarithmic derivative of γ_0 with
255 respect to volume at ambient conditions and the shear strain derivative of γ_0. The fitted parameters are
256 reported in Table 3. This model was also used to calculate the pressure of each measurement at high
257 temperature from the density and velocity data alone i.e. the absolute pressure, as reported in Table 1. A
258 more complete assessment of the pyrope equation of state can be gained by also combining data from
259 previous studies (Sinogeikin and Bass, 2002; Zou et al. 2012) where high temperature, and high
260 temperature and pressure measurements of velocities and densities were performed. Within any single
261 data set, high temperature data appear consistent with the corresponding ambient temperature data. As
262 stated previously the offset between data sets measured at ambient temperature must be due to
263 unconstrained uncertainties in the techniques employed. The magnitude of this apparent offset does not
264 appear to change, however, during heating, except in the study of Gwanmesia et al. (2006), which has

been excluded for this reason. Therefore, a single set of high temperature parameters was refined but for each data set a unique set of refined ambient temperature parameters were employed. As these high thermal parameters are highly correlated they were refined individually. The resulting "globally" fitted high thermal parameters are reported in Table 3. The parameters are similar to those proposed by Xu et al. (2008), except that the parameter η_o was found to be significantly smaller than the previously proposed value of 1. All three high-pressure data sets employed in the refinement are consistent with a value for η_o that is significantly below 1. The uncertainties on the high temperature data can be treated by considering an uncertainty of ±0.3 for both γ_o and η_o. In combination with the best fitting cold compression parameters described above, a set of "globally" fitted parameters that best describe the available experimental data are given in Table 3. Note that in Table 3 the bulk modulus and pressure derivative have been converted to the isothermal values, as required in the model of Stixrude and Lithgow-Bertelloni (2005).

Discussion

Using the same thermo-elastic parameters refined from the results of this study and the "global" fit to all applicable previous studies (Table 3), *P*- and *S*- wave velocities have been calculated for pyrope along a geotherm (Brown and Shankland 1981) at conditions corresponding to the base of the upper mantle and the transition zone (Figure 4). Furthermore the uncertainties on both pyrope models have been propagated to make an estimate of the errors when velocities are calculated at mantle conditions. These velocities are compared with the seismic reference models PREM (Dziewonski and Anderson 1981) and Ak135 (Kennett et al. 1995), as well as velocities obtained experimentally for majorite-garnet (Irifune et al. 2008), olivine and its high pressure polymorphs, wadsleyite and ringwoodite, (Duffy and Anderson 1989; Zha et al. 1998). Throughout much of this depth interval BSE or pyrolite (Ringwood 1975) bulk compositions will be composed principally of an olivine polymorph and garnet, although a few percent $CaSiO_3$ perovskite will also start to form at depths above 550 km. As can be seen there are relatively

small differences between both values and uncertainties (Figure 4) calculated with both models. For the "global" fit the uncertainties are approximately 1.5 and 2.5 % for V_p and V_s respectively, with the uncertainties arising purely from the thermal parameters being ~1 % and ~1.5 % respectively. As there seems to be no reason for excluding any of the data sets employed in the "global" fitting, the uncertainties arising from the fit must be more realistic than when a single data set is employed. Even though there are a significant number of high pressure and temperature studies on pyrope, when uncertainties are derived using the available data they are still relatively large, particularly once extrapolated to mantle conditions.

Both V_P and V_S for pyrope have a shallower gradient with depth compared to seismic models in the transition zone and are predicted to cross both PREM and Ak135 at mid transition zone conditions. Garnet formed from a bulk silicate Earth composition in the transition zone would comprise ~50 mole% of the majoritic component and also contain Fe and Ca. The velocities of such a complex majoritic garnet composition were examined experimentally by Irifune et al. (2008) up to 17 GPa and 1673K and are plotted in Figure 4 calculated along an adiabatic pressure-temperature profile across the transition zone. Both V_P and V_S for this complex garnet are significantly slower than the values determined for pyrope and are well outside of the experimental uncertainties, although potentially not outside of the combined uncertainties (Liu et al. 2015). As shown in the study of Irifune et al. (2008) most of this deviation occurs at high temperatures, as the ambient temperature elastic properties of majoritic garnets are similar to pyrope (Sinogeikin and Bass 2002). This comparison implies that the complex majoritic garnet has a value of η_o, which is at least 3 times larger than that determined here for pyrope.

As pointed out by Irifune et al. (2008) majorite garnet shear wave velocities, in particular, are significantly lower than seismic reference models towards the base of the transition zone. As the dominant mineral ringwoodite displays velocities similar to the reference models at these conditions, then a majorite-garnet bearing mantle can only have velocities significantly below the seismic reference models. The presence of ~10 % $CaSiO_3$ perovskite would not change this situation significantly. As a result it is difficult to reproduce the velocities at the base of the transition zone with a mineral model

consistent with a BSE composition at average mantle temperatures. A globally significant thermal anomaly caused by the presence of flat lying subducting slabs (Fukao et al. 2001) may be one explanation for this. Alternatively seismic reference models in the proximity of discontinuities such as that at 660 km may not reproduce average mantle velocities (Cammarano et al. 2005) due to poor constraints on the size of the discontinuity jump versus the gradient near the discontinuity. However, pyrope garnet velocities are predicted to be significantly faster than majoritic garnet. If the mantle in these regions contains above average proportions of subducted oceanic lithosphere, then the ultramafic (harzburgite) slab component would contain very little garnet, while the crustal mafic component, would be dominated by garnet with a much smaller majorite component. Such a mechanical mixture of mafic and ultramafic components may explain velocities at these depths.

Implications

The investigation of the effects of varying chemistry on garnet acoustic velocities at high pressure and temperature is key to interpreting seismic velocities at the base of the transition zone where a significant mismatch seems to occur between the observed and calculated velocities. The data and global fitting presented here provide a platform from which to construct a more comprehensive mineralogical model for complex garnets. In order for the real uncertainties to be reduced, however, it is imperative to be able to isolate the existing methodological differences that create the spread in data between various techniques. In order to minimize uncertainties in thermal parameters, which appear to dominate, it is important that acoustic measurements are performed at temperatures equal to or approaching those of the mantle.

Acknowledgements

This is Laboratory of Excellence ClerVolc contribution no. 177. Portions of this work were performed at GeoSoilEnviroCARS (Sector 13), Advanced Photon Source (APS), Argonne National Laboratory.

GeoSoilEnviroCARS is supported by the National Science Foundation - Earth Sciences (EAR-1128799) and Department of Energy - Geosciences (DE-FG02-94ER14466). Use of the Advanced Photon Source was supported by the U.S. Department of Energy, Office of Science, Office of Basic Energy Sciences, under contract DE-AC02-06CH11357. This project was also supported by ERC grant no. 227893 "DEEP" funded through the EU 7th Framework Programme. G.M.M. acknowledges funding from the French PNP program (INSU-CNRS) and Actions initiatives OPGC 2014.

References

Anderson, D.L. and Bass, J.D. (1984) Mineralogy and composition of the upper mantle. Geophysical Research Letters, 11, 637–640.

Bass, J.D., and Anderson, D.L. (1984) Composition of the upper mantle: geophysical tests of two petrological models. Geophysical Research Letters, 11, 229–232.

Brown, J. M., and Shankland T. J. (1981) Thermodynamic parameters in the Earth as determined from seismic profiles. Geophysical Journal of the Royal Astronomical Society, 66, 579–596.

Cammarano, F., Goes, S., Vacher, P., and Giardini, D. (2003) Inferring upper-mantle temperatures from seismic velocities. Physics of the Earth and Planetary Interiors, 138, 197–222.

Cammarano, F., Deuss, A., Goes, S., Giardini, D. (2005) One-dimensional physical reference models for the upper mantle and transition zone: combining seismic and mineral physical constraints. Journal of Geophysical Research 110, B01306, doi:10.1029/2004JB003272.

Chantel, J., Frost, D.J., Mc Cammon, C.A., Jing, Z., and Wang, Y. (2012) Acoustic velocities of pure and iron-bearing magnesium silicate perovskite measured to 25 GPa and 1200 K. Geophysical research letters, 39, 19.

Chen, G., Cooke Jr., J.A., Gwanmesia, G.D., and Liebermann, R.C. (1999) Elastic wave velocities of $Mg_3Al_2Si_3O_{12}$–pyrope garnet to 10 GPa. American Mineralogist, 84, 384–388.

365 Conrad, P.G., Zha, C.S., Mao, H.K., and Hemley, R.J. (1999) The high-pressure, single-crystal elasticity
366 of pyrope, grossular, and andradite. American Mineralogist, 84, 374–383.
367 Davies, G. F., and Dziewonski A.M. (1975) Homogeneity and constitution of the Earth's lower mantle
368 and outer core. Physics of the Earth and Planetary Interiors, 10, 336–343.
369 Duffy, T.S., and Anderson, D.L. (1989) Seismic velocity in mantle minerals and mineralogy of the upper
370 mantle. Journal of Geophysical Research, 94, 1895–1912.
371 Dziewonski, A.M., and Anderson, D.L. (1981) Preliminary reference Earth model. Physics of the Earth
372 and Planetary Interiors, 25, 297–356.
373 Fei, Y., Li, J., Hirose, K., Minarik, W., Van Orman, J., Sanloup, C., van Westrenen, W., Komabayashi,
374 T., and Funakoshi, K. (2004) A critical evaluation of pressure scales at high temperatures by in situ
375 X-ray diffraction measurements. Phys. Earth Planet Inter., 143/144, 516–526.
376 Fukao, Y., Widiyantoro, S., and Obayashi, M. (2001) Stagnant slabs in the upper and lower mantle
377 transition region. Reviews of Geophysics, 39, 291–323.
378 Gwanmesia G.D., and Liebermann R.C. (1993) Hot pressing of polycrystals of high pressure phases of
379 mineral phases of mantle minerals in multi-anvil apparatus. Pure and Applied Geophysics, 141, 467–
380 484.
381 Gwanmesia, G.D., Zhang, J., Darling, K., Kung, J., Li, B., Wang, L., Neuville, D., and Liebermann, R.C.
382 (2006) Elasticity of polycrystalline pyrope (Mg3Al2Si3O12) to 9 GPa and 1000C. Physics of the
383 Earth and Planetary Interiors, 155, 179–190.
384 Gwanmesia, G.D., Jackson, I., and Liebermann, R.C. (2007) In search of the mixed derivative $\delta^2 M/ \delta P \delta T$
385 (M = G, K): joint analysis of ultrasonic data for polycrystalline pyrope from gas- and solid-medium
386 apparatus. Physics and Chemistry of Minerals, 34, 85–93.
387 Irifune, T., and Ringwood, A.E. (1987) Phase transformation in primitive Morb and pyrolite compositions
388 to 25GPa and some geophysical implications. In: Manghnani, M.H., Syono, Y. (Eds.), High Pressure

389 Research in Mineral Physics, vol. 39. TERRA- PUB Tokyo/American Geophysical Union,
390 Washington, DC, pp. 235–246.
391 Irifune, T., Higo, Y., Inoue, T., Kono, Y., Ohfuji, H., and Funakoshi, K. (2008) Sound velocities of
392 majorite garnet and the composition of the mantle transition zone. Nature, 451, 814–817.
393 Ita, J., and Stixrude, L. (1992) Petrology, elasticity and composition of the transition zone. Journal of
394 Geophysical Research 81, 2483–2489.
395 Kennett, B.L.N., Engdahl, E.R., and Buland, R. (1995) Constraints on seismic velocities in the Earth from
396 travel times. Geophysical Journal International, 122, 108–124.
397 Leitner, B.J., Weidner, D.J., and Liebermann, R.C., (1980) Elasticity of single crystal pyrope and
398 implications for garnet solid solution series. Physics of the Earth and Planetary Interiors, 22, 111–
399 121.
400 Li, B., and Zhang, J. (2005) Pressure and temperature dependence of elastic wave velocity of $MgSiO_3$
401 perovskite and the composition of the lower mantle. Physics of the Earth and Planetary Interiors, 151,
402 143–154.
403 Li, B., and Liebermann, R.C. (2007) Indoor seismology by probing the Earth's interior by using sound
404 velocity measurements at high pressures and temperature. Proceedings of the National Academy of
405 Sciences of the United States of America, 104, 9145–9150.
406 Liu, Z., Irifune, T., Greaux, S., Arimoto, T., Toru, S. and Yuji, H. (2015) Elastic wave velocity of
407 polycrystalline Mj80Py20 garnet to 21 GPa and 2000K. Physics and Chemistry of Minerals, 42, 213–
408 222.
409 Matsui, M., Higo, Y., Okamoto, Y., Irifune, T., Funakoshi, K. (2012) Simultaneous sound velocity and
410 density measurements of NaCl at high temperatures and pressures: application as a primary pressure
411 standard. American Mineralogist, 97, 1670–1675.
412 Nishihara, Y., Takahashi, E. (2001) Phase relation and physical properties of an Al-depleted komatiite to
413 23 GPa. Earth and Planetary Science Letters, 190, 65–77.

O'Neill, B., Bass, J.D., Rossman, G.R., Greiger, C.A., and Langer, K. (1991) Elastic properties of pyrope. Physics and Chemistry of Minerals, 17, 617–621.

Papadakis, E.P., (1990) Ultrasonic Measurement Methods (Physical Acoustics vol XIX) eds. R.N. Thurston and A.D. Pierce (San Diego: Pierce Academic Press) 81–123.

Petricek, V., Dusek, M., and Palatinus, L. (2006) Jana2006. The crystallographic computing system. Institute of Physics, Praha, Czech Republic.

Ringwood, A. E., (1975) Composition and Petrology of the Earth's Mantle (McGraw-Hill, New York).

Saikia, A., Frost, D.J., Rubie, D.C. (2008) Splitting of the 520-kilometer seismic discontinuity and chemical heterogeneity in the mantle. Science, 319, 1515–1518.

Sammis, C., Anderson, D., and Jordan, T. (1970) Application of isotropic finite strain theory to ultrasonic and seismological data. Journal of Geophysical Research, 75, 4478–4480.

Sinogeikin, S.V., and Bass, J.D. (2000) Single-crystal elasticity of pyrope and MgO to 20 GPa by Brillouin scattering in the diamond cell. Physics of the Earth and Planetary Interiors, 120, 43–62.

Sinogeikin, S.V., and Bass, J.D. (2002) Elasticity of pyrope and majorite–pyrope solid solutions to high temperatures. Earth and Planetary Science Letters, 203, 549–555.

Stixrude, L., and Lithgow-Bertelloni, C. (2005) Thermodynamics of mantle minerals: 1. Physical properties. Geophysical Journal International, 162, 610–632.

Sumino, Y., and Nishizawa, O. (1978) Temperature variation of elastic constants of pyrope–almandine garnets. Journal of Physics of the Earth, 26, 239–252.

Suzuki, I., and Anderson, O.L. (1983) Elasticity and thermal expansion of a natural garnet up to 1000 K. Journal of Physics of the Earth, 31, 125–138.

Wang, Y., Weidner, D.J., and Guyot, F. (1996) Thermal equation of state of CaSiO3 perovskite. Journal of Geophysical Research, 101, 661–672.

Wang, Y., Rivers, M., Sutton, S., Nishiyama, N., Uchida, T., and Sanehira, T. (2009) The large-volume high pressure facility at GSECARS: A "Swiss-army-knife" approach to synchrotron-based experimental studies. Physics of the Earth and Planetary Interiors, 174, 1–4, 270–281.

Weidner, D.J., and Ito, E. (1987) Mineral physics constraints on a uniform mantle composition. In: Manghnani, M.H., Syono, Y. (Eds.), High Pressure Research in Mineral Physics, vol. 39. TERRA-PUB Tokyo/American Geophysical Union, Washington, DC, pp. 439–446.

Xu, W., Lithgow-Bertolini, C., Stixrude, L., and Ritsema, J. (2008) The effect of bulk composition and temperature on mantle seismic structure. Earth and Planetary Science Letters, 275, 70–79.

Zha, C.S., Duffy, T.D., Downs, R.T., Mao, H.K., Hemley, R.J. (1998) Brillouin scattering and X-ray diffraction of San Carlos olivine: direct pressure determination to 32 GPa. Earth and Planetary Science Letters, 159, 25–33.

Zou, Y., Irifune, T., Steeve, G., Whitaker, M.L., Shinmei, T., Ohfuji, H., Negishi, R. and Higo, Y. (2012) Elasticity and sound velocities of polycrystalline Mg3Al2(SiO4)3 garnet up to 20 GPa and 1700 K, Journal of Applied Physics, 112, 014910, doi:10.1063/1.4736407.

Figure captions

Figure 1: Scanning electron microscope images of the polycrystalline pyrope sample. Grains are texturally well equilibrated and there is no evidence of porosity or secondary phases in the sample. The grain size is in the range 2 to 5 μm.

Figure 2: Compressional (*P*) and shear (*S*) wave velocities of pyrope from this study determined at ambient temperature (green dots), as a function of "absolute" pressure, determined from equation 13. Solid black triangles and squares are data from Sinogeikin and Bass (2000) and Zou et al. (2012) respectively. Open triangles and squares are data from Gwanmesia et al. (2006, 2007) and Chen et al. (1999) respectively.

462

463 **Figure 3**: Compressional and shear wave velocities of pyrope garnet as a function of the absolute
464 pressures (see main text) and temperature. The colored dots show the velocities from the present study at
465 five different temperatures. The two curves are determined using the thermo-elastic model (Table 3) fitted
466 to this study, calculated at ambient temperature (green) and 1300 K (red). Black squares show the data of
467 Zou et al. (2012) for a similar pyrope sample and the black diamonds are from the study of Irifune et al.
468 (2008) for a majoritic garnet formed in a natural chemical system. Open symbols refer to high
469 temperature data and the conditions of both studies are indicated in the legend.

470

471 **Figure 4**: A comparison of sound velocities for pyrope and other relevant high-pressure phases in the
472 mantle transition zone with the seismological models PREM (Dziewonski and Anderson 1981) and
473 Ak135 (Kennett et al. 1995). Solid lines are the calculated velocity changes along a mantle adiabat for
474 pyrope (green, fit from this study and dark blue, "global" fit to all suitable studies) with the associated
475 uncertainties (faded green and blue areas). Curves for olivine and its high-pressure polymorphs (red)
476 (Duffy and Anderson 1989; Zha et al. 1998), majorite (light blue) (Irifune et al. 2008) and $CaSiO_3$-
477 perovskite (Wang et al. 1996) have been calculated by fitting the available experimental data using the
478 model of Stixrude and Lithgow-Bertelloni (2005). Arrows indicate the depths at which phase transitions
479 in major minerals take place in a BSE mineralogical model. Py = pyrope; Ol = olivine; Wd = wadsleyite;
480 Rw = ringwoodite; Mj = majorite garnet; CaPv = $CaSiO_3$-rich perovskite.

481

482 **Supplementary Figure 1**: Schematic cross section of the 10mm multi-anvil cell assembly used for the
483 ultrasonic measurement experiments.

484

485 **Supplementary Figure 2**: X-ray images of a sample recorded up to the maximum pressure of 23.8 GPa,
486 according to the Au pressure scale, and at various temperatures during the heating cycle up to 1300K.

From the bottom: Al_2O_3 buffer rod, Au foil, sample, Au foil and NaCl. Inclined dark shadows are caused by the opaque WC anvils.

Supplementary Figure 3: MHz - pulse echoes from ultrasonic experiments performed at high and low pressures.

Tables

Table 1: Velocity and density data collected for pyrope.

P (GPa)	Abs. P (GPa)	T (K)	V_P (km.s^{-1})	V_S (km.s^{-1})	ρ (g.cm^{-3})
RP*	RP*	298			3.565(4)
2.3	2.0	298	9.16(5)	5.10(3)	3.607(4)
5.7	5.2	298	9.40(5)	5.16(3)	3.668(4)
7.5	6.9	298	9.53(5)	5.20(3)	3.701(4)
9.8	9.2	298	9.68(5)	5.25(3)	3.742(4)
12.5	12.0	298	9.85(5)	5.33(3)	3.791(4)
15	14.7	298	10.02(5)	5.39(3)	3.836(4)
17.6	17.7	298	10.19(5)	5.47(3)	3.883(5)
19.4	19.8	298	10.31(5)	5.53(3)	3.916(4)
21.5	22.3	298	10.42(5)	5.59(3)	3.954(4)
23.8	25.2	298	10.53(5)	5.64(3)	3.996(4)
23	24.2	373	10.45(5)	5.61(3)	3.978(5)
21.9	23.0	473	10.36(5)	5.56(3)	3.955(5)
21.8	23.2	573	10.30(6)	5.51(4)	3.952(4)
20.1	20.0	1273	10.08(8)	5.41(5)	3.854(4)
19.1	19.2	1273	10.02(8)	5.38(5)	3.841(5)

*Ambient pressure. Abs. refers to absolute pressure determined using equation 15 and at high temperature from the model parameters given in table 3 for this study. Data were collected during cooling and decompression but are reported in the opposite order.

This is a preprint, the final version is subject to change, of the American Mineralogist (MSA)
Cite as Authors (Year) Title. American Mineralogist, in press.
(DOI will not work until issue is live.) DOI: http://dx.doi.org/10.2138/am-2016-5335

503 **Table 2**: Pyrope bulk and shear moduli and their pressure and temperature derivatives

Study	P_{max} (GPa)	K_{S0} (GPa)	K' (GPa)	$(\delta K_S/\delta T)_P$ (MPa/K)	G_0 (GPa)	G' (GPa)	$(\delta G/\delta T)_P$ (MPa/K)
Ultrasonic interferometry							
This study	23.8	172 (±1.6)	4.38 (±0.08)	-17.8 (±2.0)	89.1 (±0.5)	1.66 (±0.05)	-7.9 (±1.0)
Chen et al. (1999)	10	171.0 (±2.0)	5.3 (±0.4)		92.0 (±1.0)	1.6 (±0.2)	
Gwanmesia et al. (2006)	8.7	175.0 (±2.0)	3.9 (±0.3)	-18.0 (±2.0)	91.0 (±1.0)	1.7 (±0.2)	-10.0 (±1.0)
Gwanmesia et al. (2007)	0.3	166.0 (±0.2)		-19.3 (±0.4)	92.2 (±1.0)		-10.4 (±0.2)
Zou et al. (2012)	19.86	170.0 (±0.2)	4.51 (±0.2)	-17.0 (±2.0)	93.2 (±0.1)	1.51 (±0.2)	-10.7 (±1.0)
Brillouin scattering							
Sinogeikin and Bass (2000)	20	171.2 (±2.0)	4.1 (±0.3)	-14.0 (±2.0)	93.7 (±2.0)	1.3 (±0.2)	-9.2 (±1.0)
Conrad et al. (1999)	8.75	172.7	3.2		92	1.4	
Leitner et al. (1980)	0	177.0 (±1.0)			89.0 (±1.0)		
O'Neill et al. (1991)	0	172.8 (±0.3)			92.0 (±0.2)		

504

505

506 **Table 3:** Thermo-elastic parameters.

	K_{T0}	G_{T0}	K'_{T0}	G'_0	γ_o	q	θ	η_o
This study	170.8±1.5	89.1±0.5	4.43±0.08	1.66±0.05	1.15±0.3	1.5	823	0.45±0.3
Global fit	169.5±2.6	91.4±0.6	4.38±0.2	1.55±0.1	1.15±0.3	1.5	823	0.45±0.3

507 The "Global fit" is obtained by simultaneously fitting data from this study, Sinogeikin and Bass (2000; 2002) and Zou et al.

508 (2012) in addition to the ambient temperature data of Gwanmesia et al. (2006).

This is a preprint, the final version is subject to change, of the American Mineralogist (MSA)
Cite as Authors (Year) Title. American Mineralogist, in press.
(DOI will not work until issue is live.) DOI: http://dx.doi.org/10.2138/am-2016-5335

Figure 1

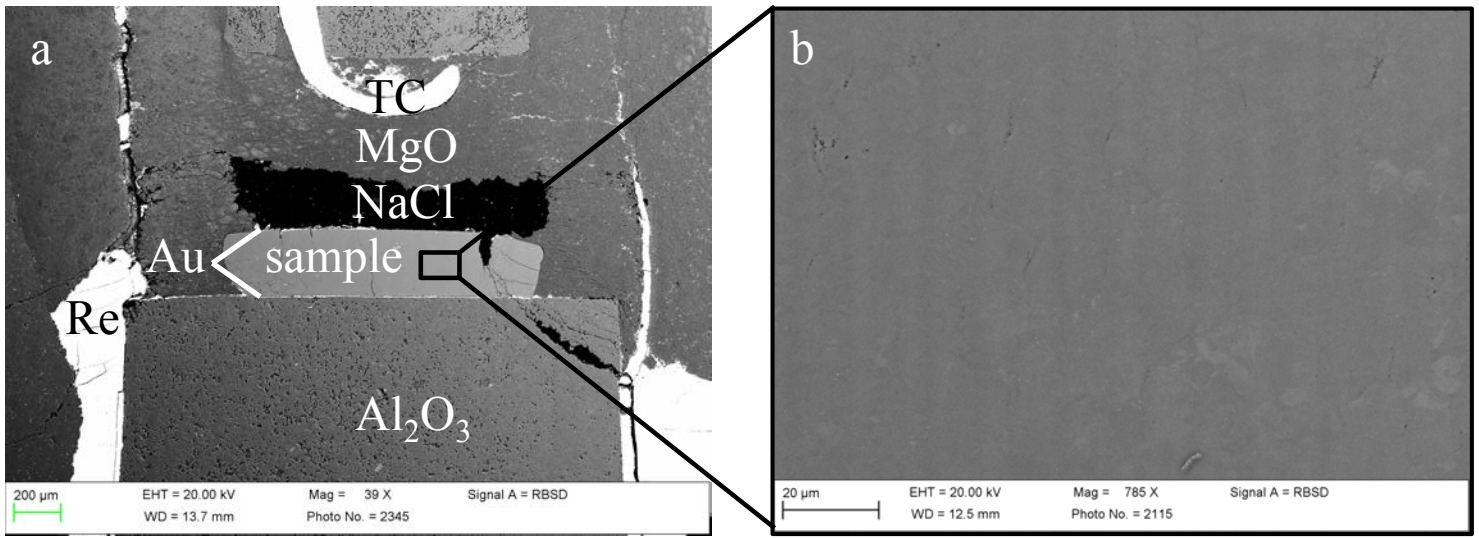

This is a preprint, the final version is subject to change, of the American Mineralogist (MSA)
Cite as Authors (Year) Title. American Mineralogist, in press.
(DOI will not work until issue is live.) DOI: http://dx.doi.org/10.2138/am-2016-5335

Figure 2

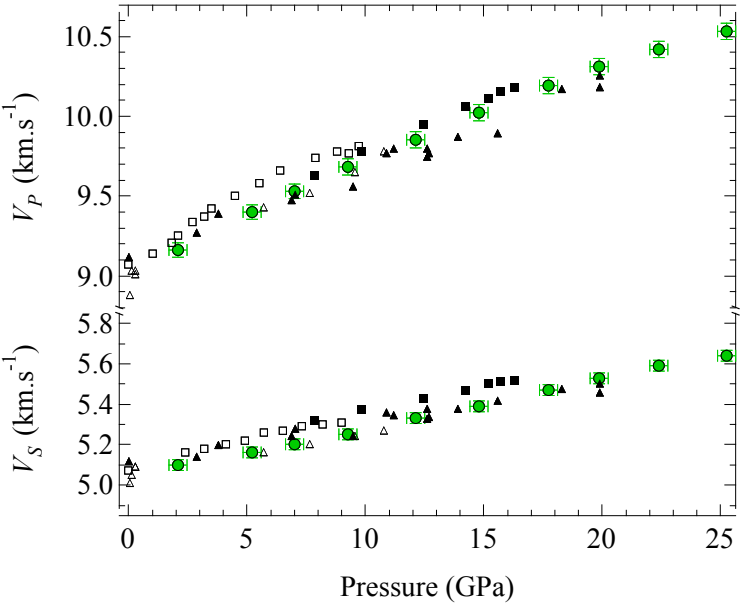

This is a preprint, the final version is subject to change, of the American Mineralogist (MSA)
Cite as Authors (Year) Title. American Mineralogist, in press.
(DOI will not work until issue is live.) DOI: http://dx.doi.org/10.2138/am-2016-5335

Figure 3

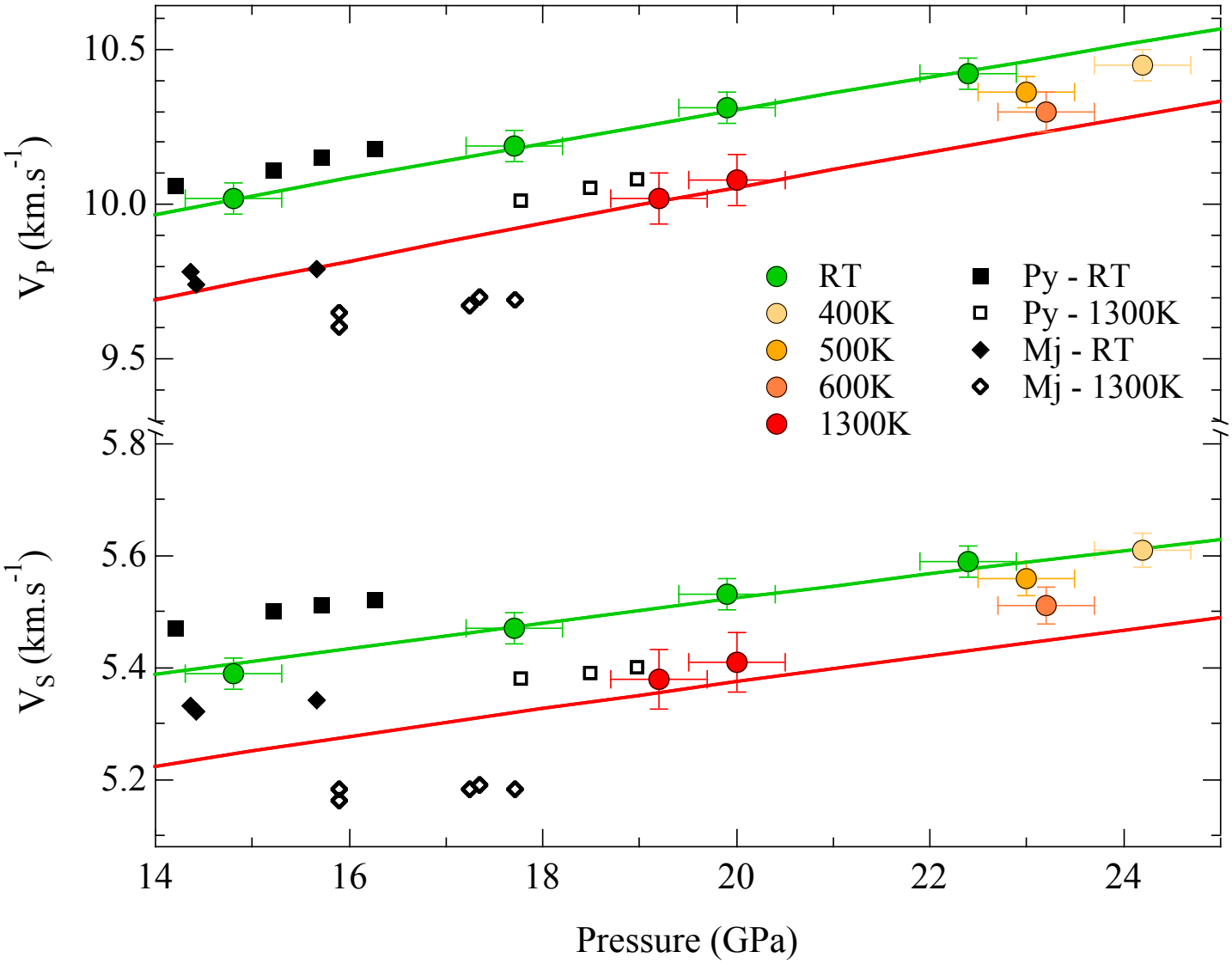

This is a preprint, the final version is subject to change, of the American Mineralogist (MSA)
Cite as Authors (Year) Title. American Mineralogist, in press.
(DOI will not work until issue is live.) DOI: http://dx.doi.org/10.2138/am-2016-5335

Figure 4